

## Surface stress effects on the bending properties of fcc metal nanowires

Geng Yun and Harold S. Park\*

*Department of Mechanical Engineering, University of Colorado, Boulder, Colorado 80309, USA*

(Received 10 November 2008; revised manuscript received 24 March 2009; published 19 May 2009)

The major purpose of this work is to investigate surface stress effects on the bending behavior and properties of  $\langle 100 \rangle / \{100\}$  gold nanowires with both fixed/fixed and fixed/free boundary conditions. The results are obtained through utilization of the recently developed surface Cauchy-Born model, which captures surface stress effects on the elastic properties of nanostructures through a three-dimensional, nonlinear finite element formulation. There are several interesting findings in the present work. First, we quantify the stress and displacement fields that result in the nanowires due to bending deformation. In doing so, we find that regardless of boundary condition, the stresses that are present in the nanowires due to deformation induced by surface stresses prior to any applied bending deformation dominate any stresses that are generated by the bending deformation unless very large ( $\approx 5\%$ ) bending strains are applied. In contrast, when the stresses and displacements induced by surface stresses prior to bending are subtracted from the stress and displacement fields of the bent nanowires, we find that the bending stresses and displacements do match the solutions expected from bulk continuum beam theory, but only within the nanowire bulk, and not at the nanowire surfaces. Second, we find that the deformation induced by surface stresses also has a significant impact on the nanowire Young's modulus that is extracted from the bending simulations, where a strong boundary-condition dependence is also found. By comparing all results to those that would be obtained using various linear surface-elastic theories, we demonstrate that a nonlinear, finite deformation formulation that captures changes in both bulk- and surface-elastic properties resulting from surface stress-induced deformation is critical to reproducing the experimentally observed boundary-condition dependence in Young's modulus of metal nanowires. Furthermore, we demonstrate that linear surface-elastic theories based solely on the surface energy erroneously predict an increase in Young's modulus with decreasing nanowire size regardless of boundary condition. In contrast, while the linear surface-elastic theories based upon the Gurtin and Murdoch formalism can theoretically predict elastic softening with decreasing size, we demonstrate that, regardless of boundary condition, the stiffening due to the surface stress dominates the softening due to the surface stiffness for the range of nanowire geometries considered in the present work. Finally, we determine that the nanowire Young's modulus is essentially identical when calculated via either bending or resonance for both boundary conditions, indicating that surface effects have a similar impact on the elastic properties of nanowires for both loading conditions.

DOI: [10.1103/PhysRevB.79.195421](https://doi.org/10.1103/PhysRevB.79.195421)

PACS number(s): 61.46.-w, 62.25.-g, 68.35.Gy, 68.65.-k

### I. INTRODUCTION

Nanowires have been intensely researched by both the scientific and engineering communities over the past decade.<sup>1-3</sup> One of the major reasons for the surge in interest for nanowires has been due to their potential as the basic building block for nanoelectromechanical systems (NEMS). As the basic building block for NEMS, nanowires will be used to perform chemical sensing, act as high-frequency oscillators, used to perform ultrasensitive mass and force detection, and to act as next generation wireless components.<sup>4-6</sup> Of relevance to the present study, in many NEMS applications, nanowires will be synthesized and actuated in beamlike geometries and configurations that appear amenable to description using standard continuum beam theory.

Due to the fact that nanowires have beamlike geometries and because many of the potential NEMS applications require knowledge of the nanowire elastic properties, there has been a recent surge of interest in both experimental and theoretical techniques to characterize the elastic properties of nanowires. The experimental characterization has typically involved two distinct experimental techniques, those utilizing atomic force microscope (AFM)-induced bending,<sup>7-14</sup>

and those utilizing resonance-based measurements.<sup>15-21</sup> Unfortunately, there is significant scatter in the experimental results,<sup>3</sup> with some reporting an enhanced elastic stiffness,<sup>10,11,18</sup> some reporting a reduced elastic stiffness,<sup>17,21-23</sup> and some reporting no variation in elastic stiffness<sup>8,9,13,14</sup> with decreasing nanostructure size. We note that the cross-sectional sizes of these nanowires typically are in the range of 50–250 nm, where nanoscale size and surface effects may be limited.

The size dependence in elastic behavior and properties at the nanoscale arises due to surface stress<sup>24-27</sup> and surface-elastic effects,<sup>28-30</sup> both of which occur due to the reduced coordination number<sup>31</sup> that characterizes surface atoms as compared to those that lie within the material bulk. Furthermore, the percentage of surface atoms, and therefore the percentage of atoms that have a reduced coordination number increases with the increasing surface area to volume ratio that is characteristic of nanomaterials. Because the surface effects are related to surface area to volume ratio, the surface stress and surface-elastic effects become significant with decreasing structural size.

Atomistic modeling has predicted a strong size dependence in the elastic properties of nanostructures at cross-sectional sizes smaller than about 10 nm.<sup>28,29,32-35</sup> However, most atomistic calculations have been performed considering

axial tensile loading, while comparably few results exist for bending.<sup>36–38</sup> This fact is critical because as is well known, the surfaces of beams are subject to the maximum tensile and compressive states of stress under bending. Because surfaces are the key factor in altering the elastic properties of nanostructures, it is likely that the elastic properties of nanowires measured under bending may differ from those measured under resonance or axial testing approaches.<sup>39</sup>

The theoretical models that have been developed for nanostructures are typically based upon further developments of the linear surface-elastic theory of Gurtin and Murdoch,<sup>40</sup> which treats the surface as a deformable elastic medium attached to the bulk and which can be described using a Hooke’s-law-type linear elastic stress strain relationship. Various surface-elastic models have been developed<sup>30,39,41–46</sup> and utilized to study the effects of surfaces on the bending behavior and properties of nanowires. There are several key shortcomings of these models that have motivated the present work. In particular, (1) the models are generally two-dimensional (2D), which neglects the changes in cross-sectional area that arise due to the deformation induced by surface stresses,<sup>25–27</sup> (2) some models assume that surface physics can be captured using overly simplistic interatomic pair potentials to describe the surface bond energetics; these are physically incorrect because pair potentials predict that the surface stress of metals is compressive rather than tensile, (3) the complex nature of the analytic equations makes these models difficult to implement in finite element (FE)-type numerical analysis, (4) due to equilibrium requirements enforced between the bulk and surface in deriving the surface-elastic formulation,<sup>24,40</sup> the surface stress in the surface-elastic formulation is a  $2 \times 2$  *in-plane* stress tensor, where the out-of-plane stress component must be zero to satisfy the mechanical equilibrium condition. The implication of this  $2 \times 2$  in-plane surface stress tensor is that surface-elastic formulations are unable to capture the surface-stress-driven compressive relaxation that metal nanowires are known to undergo.<sup>25–27</sup> (5) Due to the linear elastic constitutive response that is assumed for both the bulk and surface, the surface-elastic models are unable to capture the nonlinear elasticity of the nanowire bulk which results due to surface stress driven compressive strain, and which is known to play a critical role in the elastic properties of metal nanowires,<sup>29</sup> (6) The stress and displacement fields in the nanowires have not been quantified to date for different boundary conditions while accounting for surface stress-induced deformation using a nonlinear, finite deformation constitutive model.

In the present work, we utilize the recently developed surface Cauchy-Born (SCB) model,<sup>47,48</sup> which captures the bulk and surface-elastic properties of nanostructures directly from an underlying atomistic potential<sup>49,50</sup> using nonlinear, finite deformation kinematics to study surface stress effects on the bending behavior and properties of  $\langle 100 \rangle$  gold nanowires with  $\{100\}$  transverse surfaces. We focus upon intermediate-size nanowires, with cross-sectional dimensions between 15 and 25 nm, in order to bridge the small size scales that have been studied atomistically, and the larger sizes that have been evaluated experimentally.

By considering nanowires of varying cross-sectional area and aspect ratio, using both fixed/free and fixed/fixed bound-

ary conditions, we arrive at the key findings of the present work, which are: (1) corresponding to the discussion above regarding the inability of current surface-elastic formulations to capture surface-stress-driven relaxation of the nanowires, we find that the stresses and displacements induced in the nanowires due to surface-stress-driven relaxation are significantly larger than the stresses and displacements induced by bending of the nanowires, even out to large ( $>1\%$ ) bending strains and for fairly large nanowire cross sections ( $>25$  nm). (2) The bending stiffness, and therefore Young’s modulus of the nanowires is strongly boundary condition and size dependent. We discuss the implications of these findings, and compare our results to previous analytic results based upon linear surface elasticity for nanowire bending<sup>10,11,42</sup> to demonstrate how and why our findings are different from those found using either linear continuum beam theory or linear surface-elasticity theory. Finally, we compare results for the nanowire Young’s modulus obtained via bending in the present work to resonance<sup>51</sup> to determine if there are any quantifiable differences induced by the testing or loading method in how surfaces impact the nanowire Young’s modulus.

## II. SURFACE CAUCHY-BORN MODEL

### A. Overview

The standard bulk Cauchy-Born (BCB) model is a multi-scale, finite deformation constitutive model that enables the calculation of continuum stress and stiffness directly from an underlying interatomic potential energy.<sup>52–57</sup> However, because the BCB model does not account for critical nanoscale surface stress effects, the SCB model was recently developed by Park *et al.*<sup>47,48,55</sup> to capture surface stress effects within the framework of the Cauchy-Born approximation. Because the SCB formulation for FCC metals was presented in previous works by Park *et al.*,<sup>48,51</sup> we refer the interested reader to those works for a detailed exposition on the SCB model.

As noted in previous expositions on the SCB model for FCC metals,<sup>48,51</sup> the SCB model is based on constructing a surface strain energy density  $\gamma(\mathbf{C})$  of a representative surface unit cell, where  $\mathbf{C} = \mathbf{F}^T \mathbf{F}$  is the continuum stretch tensor, indicating that the SCB model is a nonlinear, finite deformation model. The surface energy density  $\gamma(\mathbf{C})$  is calculated in the present work using the embedded atom (EAM) potential for gold of Foiles.<sup>50</sup>

We note that extensive studies comparing the SCB model and purely atomistic simulations for the surface-stress-driven relaxation of fixed/free FCC metal nanowires have been performed using EAM potentials by Park and Klein;<sup>48</sup> the accuracy of the SCB model in predicting the compressive relaxation strain of the free end was found to be less than 10% for nanowire cross-sectional sizes larger than about 8 nm. We also note that the EAM potentials utilized in the present work are well known to underestimate both the surface energy and surface stress by 30–50% as compared to DFT calculations or experiments;<sup>58</sup> these errors are transferred to the SCB model because it is based upon the EAM potentials.

We also emphasize the differences between the SCB formulation for surface stress and surface energy, and the tradi-

tional thermodynamic definition of surface stress (see for example<sup>24,59</sup>),

$$\tau = \tau_0 + \mathbf{C}_0 \epsilon, \tag{1}$$

where  $\tau$  is the surface stress,  $\tau_0$  is the residual (strain-independent) portion of the surface stress,  $\mathbf{C}_0 \epsilon$  is the surface-elastic (strain-dependent) part of the surface stress, and where  $\mathbf{C}_0$  is the (constant) surface-elastic stiffness. Interestingly, recent works by Park and Klein<sup>51</sup> and Park<sup>60</sup> have demonstrated that if finite deformation kinematics is considered, as they are in the SCB model, the residual surface stress  $\tau_0$  does in fact contribute significantly to the resonant frequencies of both metallic and semiconducting nanowires.

The difference is that the SCB surface energy density  $\gamma(\mathbf{C})$  represents the actual surface energy of the surface unit cell, and not the excess in energy as compared to a representative bulk atom, which is how the surface energy is traditionally defined thermodynamically.<sup>24</sup> Once the surface energy density is known, the second surface Piola-Kirchhoff stress and the surface stiffness can be calculated by taking derivatives of the surface energy density  $\gamma(\mathbf{C})$  with respect to the stretch tensor  $\mathbf{C}$  [see Eq. 12 in Park and Klein<sup>48</sup>].

### III. NUMERICAL EXAMPLES

All numerical examples were performed on three-dimensional, single-crystal gold nanowires of length  $L$  and

TABLE I. Summary of nanowire geometries considered: constant aspect ratio, and constant cross-sectional area. All dimensions are in Angstroms (Å).

CAR	CCSA
1200 × 150 × 150	1280 × 160 × 160
1440 × 180 × 180	2560 × 160 × 160
1680 × 210 × 210	3840 × 160 × 160
1920 × 240 × 240	4800 × 160 × 160

square cross section of width  $a$ . Two different parametric studies are conducted in this work, which consider nanowires with constant cross-sectional area (CCSA), where  $a = 160$  Å, and constant aspect ratio (CAR) of  $L/a=8$ ; the geometries are summarized in Table I. All simulations were performed using the Sandia-developed simulation code Tahoe.<sup>61</sup>

All wires had a  $\langle 100 \rangle$  longitudinal orientation with  $\{100\}$  transverse surfaces, while two different boundary conditions, fixed/free and fixed/fixed ends were used; we note that these boundary conditions are similar to what has been assumed in both experimental<sup>10,11,14</sup> studies and theoretical<sup>10,11</sup> studies of nanowire bending, to which we will compare the obtained SCB results in Sec. VI. All finite element (FE) simulations were performed using the stated boundary conditions and utilized regular meshes of eight-node hexahedral elements,

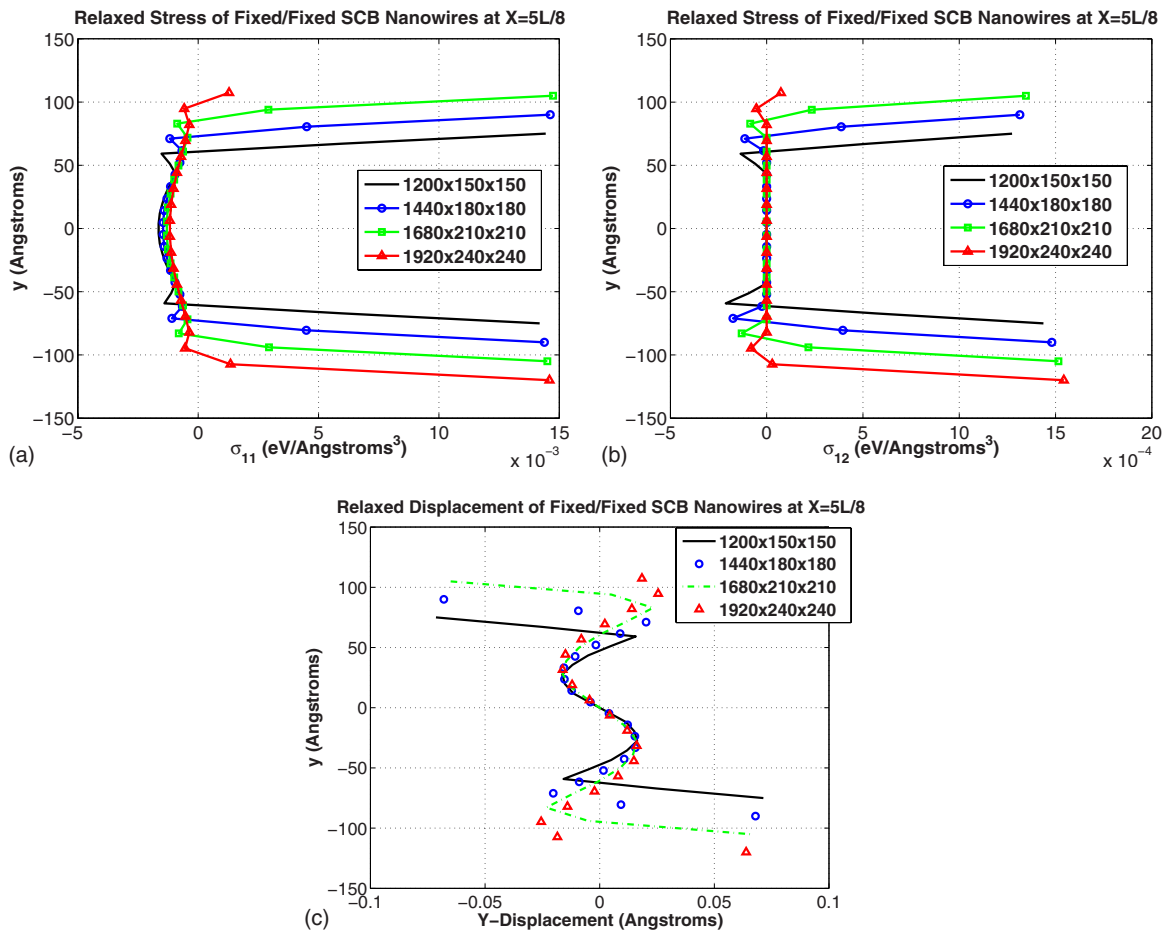


FIG. 1. (Color online) Stresses and  $y$  displacements in CAR fixed/fixed nanowires after deformation due to surface stresses.

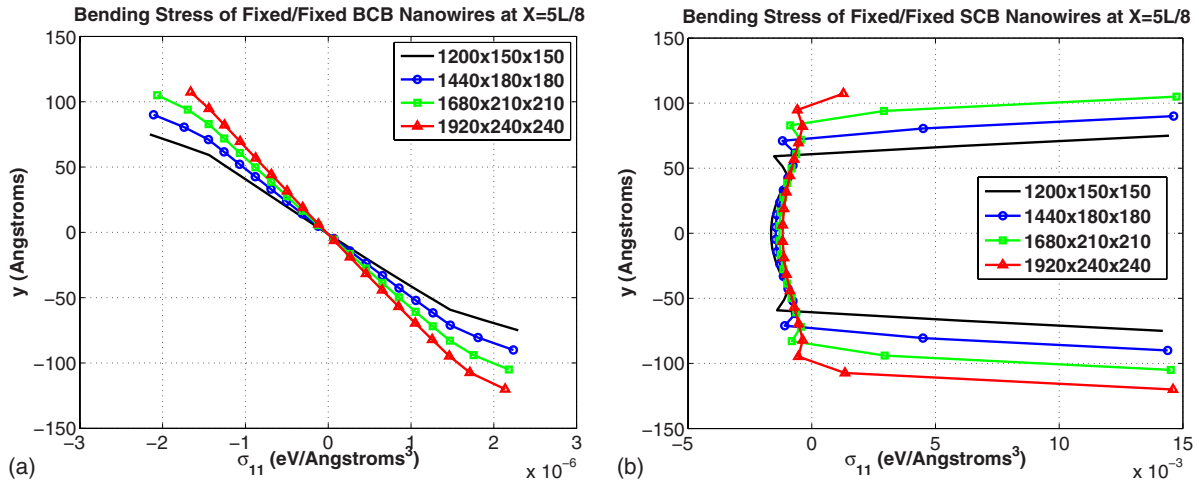


FIG. 2. (Color online) Bending  $\sigma_{11}$  for BCB and SCB CAR fixed/fixed nanowires.

with at least ten finite elements through the nanowire thickness.

Regardless of whether fixed/free or fixed/fixed boundary conditions are utilized, the nanowires are initially out of equilibrium due to the surface stresses. Therefore, before any external bending deformation was applied, we first determined the minimum energy, or relaxed configurations of the nanowires due to the surface stresses. Finding the minimum-energy configurations corresponds directly to what would occur experimentally, in which the nanowires deform in response to surface stresses after the synthesis or etching process.

Once the minimum-energy configuration due to surface stresses was determined, external loading was applied incrementally under quasistatic loading, such that the nanowire could equilibrate due to a given load increment before additional loading was applied. The elastic properties and the bending stresses were determined after applying bending strains of  $8.5e-3\%$  for the CAR nanowires and  $8.6e-2\%$  for the CCSA nanowires; however, additional calculations were carried out where the nanowires were bent to strains nearing 5%. In all cases, we also performed the simulations using the BCB model, i.e., without surface stresses, to quantify how

surface stresses cause variations in both the nanowire elastic properties, as well as the stress and displacement fields, as a function of size.

#### IV. STRESS AND DISPLACEMENT FIELD IN THE NANOWIRE AFTER SURFACE STRESS INDUCED DEFORMATION

Before discussing the bending-induced stresses and displacements in the nanowires, we first discuss the state of stress and the displacement fields that occur in the nanowires as a result of surface stress-induced deformation, i.e., in the absence of any applied external forces, as we will demonstrate that this is critical to the understanding of nanowire bending stresses, deformation, and elastic properties. As discussed earlier, the nanowires are initially out of equilibrium due to the surface stresses, and therefore deform in response to the surface stresses until an equilibrium configuration is reached in which the tensile surface stresses are balanced by compressive stresses within the nanowire bulk.

While both fixed/fixed and fixed/free CCSA and CAR nanowires were considered, we focus on the fixed/fixed CAR nanowires as the other geometries and boundary conditions

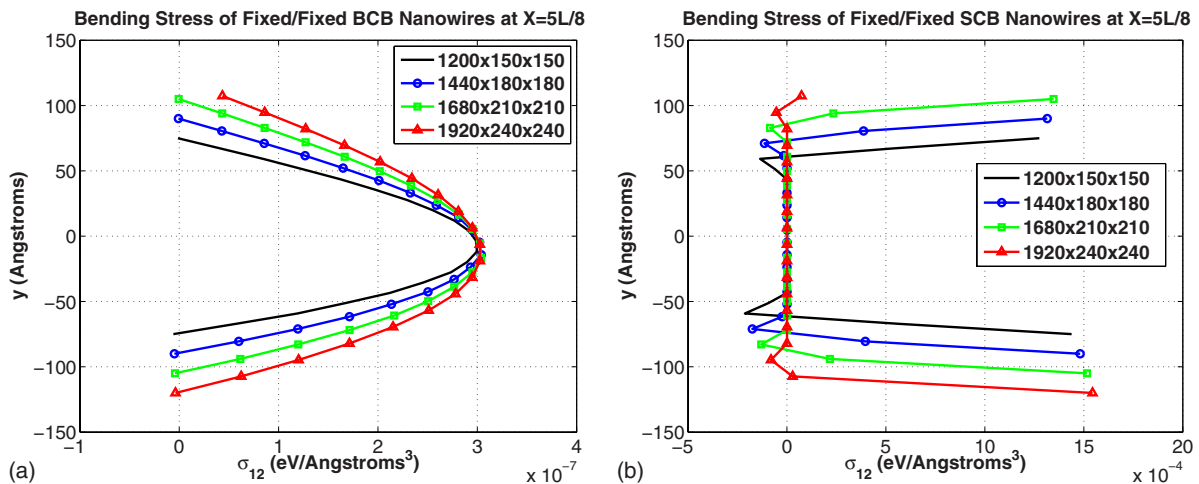


FIG. 3. (Color online) Bending  $\sigma_{12}$  for BCB and SCB CAR fixed/fixed nanowires.

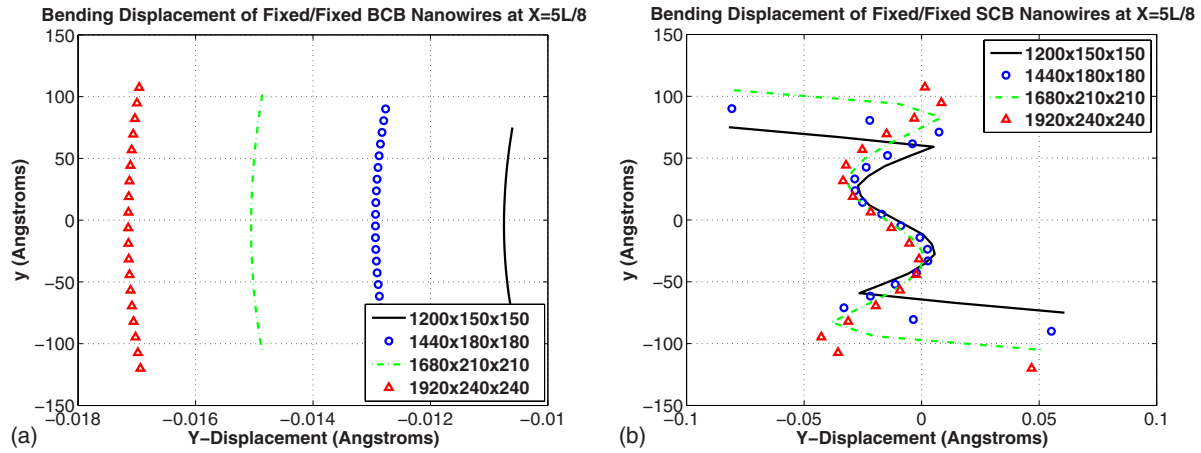


FIG. 4. (Color online) Bending ( $y$ ) displacement across the cross section for fixed/fixed CAR nanowires after bending force has been applied for both BCB and SCB nanowires.

lead to similar conclusions regarding surface stress effects on the displacements and stresses in the nanowires. The stresses in the fixed/fixed CAR nanowires after surface-stress-driven relaxation are shown in Fig. 1. For the normal stress  $\sigma_{11}$ , we first note that  $\sigma_{11}$  is positive at the nanowire surfaces but negative within the nanowire core. The normal stress  $\sigma_{11}$  is positive at the free surfaces of the nanowire due to the tensile nature of metallic surface stresses.<sup>58</sup> In general,  $\sigma_{11}$  is larger at the surfaces for fixed/fixed nanowires due to the fact that the fixed/free nanowires can contract axially and thereby relieve some of the effects of the tensile surface stress.

In contrast,  $\sigma_{11}$  is negative within the nanowire bulk for both boundary conditions; it is negative for the fixed/fixed case because while both ends of the nanowire are fixed, the interior still relaxes and compresses slightly in response to the surface stresses. The size-dependent effect of the surface stresses reveals itself in the normal stresses  $\sigma_{11}$  in Fig. 1. For the fixed/fixed CAR nanowires in Fig. 1, there is a slight difference in  $\sigma_{11}$  between the largest nanowire with cross-sectional length 24 nm, and the smallest, with cross-sectional length of 15 nm;  $\sigma_{11} = -0.0012 \text{ eV}/\text{\AA}^3$  for the 24 nm CAR nanowire, while  $\sigma_{11} = -0.0016 \text{ eV}/\text{\AA}^3$ , or about  $-0.25 \text{ GPa}$ , for the 15 nm CAR nanowire. While the fixed ends prevent the nanowire from contracting along its length, the smaller 15 nm CAR nanowire experiences slightly more bulk compression due to surface stresses, and thus is subject to a larger compressive  $\sigma_{11}$ .

In contrast to the normal stress  $\sigma_{11}$ , the shear stress  $\sigma_{12} = 0$  in the interior of the nanowires, regardless of the boundary condition. On the surfaces of the nanowires, the nature of the shear stress depends upon the state of surface deformation;  $\sigma_{12}$  is positive in Fig. 1 at the surfaces because the surfaces are in tension resulting from the fixed end boundary conditions.

Regarding the displacement field, for the fixed/fixed nanowire in Fig. 1, we note that the vertical ( $y$ ) displacements are negative at the top surface and positive at the bottom surface, indicating that the cross-sectional area has contracted in response to the surface stresses.

Before moving forward to discuss the effects of bending forces on the nanowire state of stress, we re-emphasize that

the results shown in Fig. 1 constitute the state of stress and the vertical ( $y$ )-displacement field in the nanowires *before* any externally applied forces to induced bending are applied.

## V. NANOWIRE BENDING STRESS AND DISPLACEMENT RESULTS

We now discuss the actual bending stresses and displacements for the CAR nanowires, for both fixed/fixed and fixed/free boundary conditions. Again, we emphasize that the bending forces were applied *after* the nanowires were allowed to find a minimum-energy configuration due to the surface stresses, as was discussed in the previous section. We show results for both SCB and BCB (i.e., without surface stress effects) CAR nanowires to compare how the bending stresses of nanowires are different when surface stresses are accounted for.

The stress in the nanowire after bending for the fixed/fixed BCB and SCB CAR nanowires is shown in Figs. 2 and 3. As can be seen, the BCB nanowire stresses exhibit the expected trends from continuum beam theory, i.e.,  $\sigma_{11}$  is linear, as seen in Fig. 2, and  $\sigma_{12}$  is parabolic, as seen in Fig. 3. However, the bending stresses for the SCB nanowire are quite different. As seen in Figs. 2 and 3, the normal stress  $\sigma_{11}$  does not exhibit a linear pattern, nor does the shear stress  $\sigma_{12}$  exhibit a parabolic pattern. In fact, the bending stresses for the SCB nanowires appear to be remarkably similar to the stresses present in the nanowires due to surface-stress-induced deformation as previously seen in Fig. 1 for fixed/fixed CAR nanowires.

Similarly, a comparison between the  $y$ -displacement field after bending at the center of the fixed/fixed beam for SCB and BCB nanowires is shown in Fig. 4. While the BCB displacement field is parabolic, and slightly negative due to the applied force, the displacement field in the SCB nanowire is significantly different. There, the top surface has a significantly larger downward displacement than the bottom surface, and there is an oscillation of the displacement field between the two surfaces. Furthermore, the SCB displacement field in Fig. 4 appears as though it can be obtained by

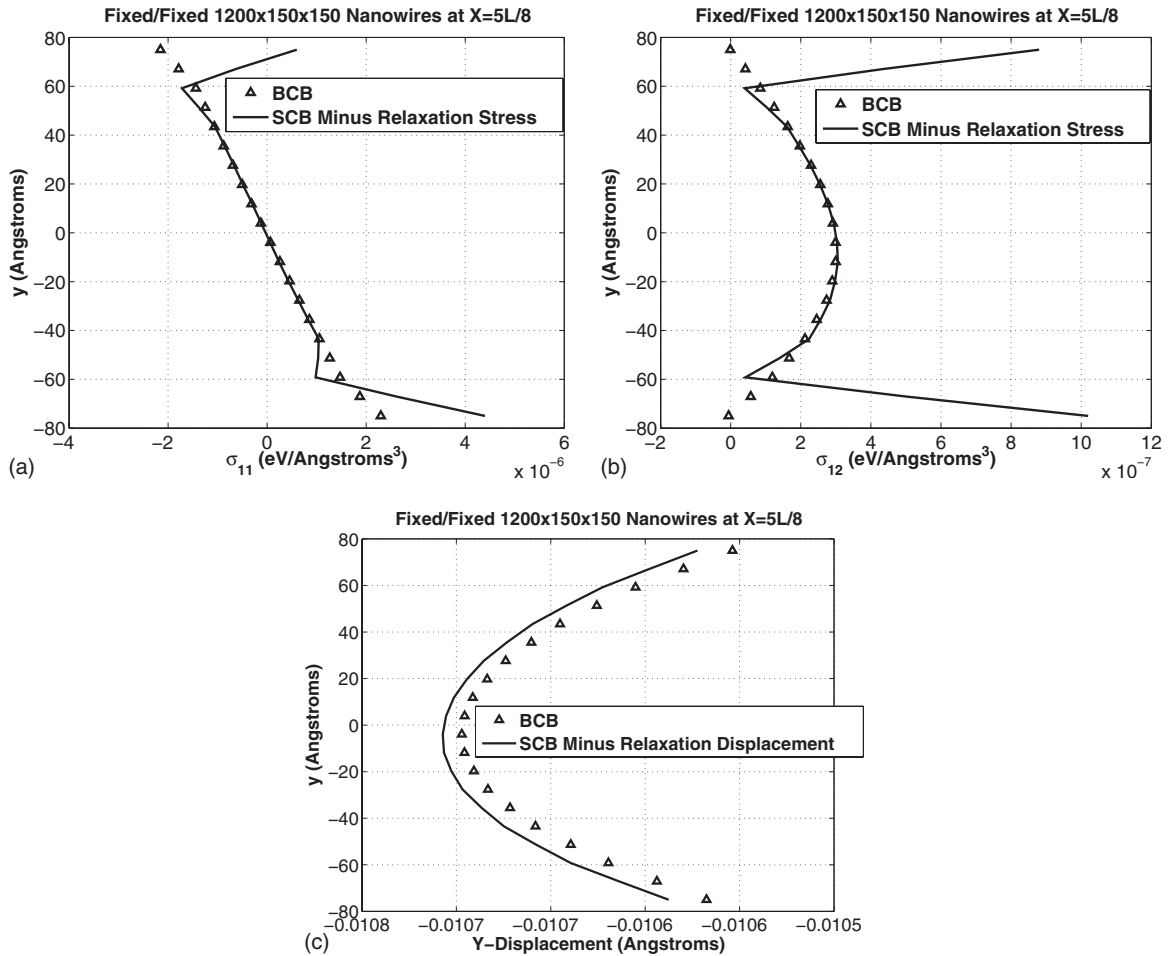


FIG. 5. Bending stresses and (y) displacement across the cross section for CAR nanowires after relaxation stress and displacement in Fig. 1 has been subtracted from SCB bending results in Figs. 2–4.

adding the relaxed SCB displacement field in Fig. 1 and the BCB bending displacement field in Fig. 4.

Due to the similarity between the bending stresses in Figs. 2 and 3, and the relaxed stresses (i.e., the stresses due to deformation induced by surface stresses before the application of any external bending forces) in Fig. 1, and also between the bending displacements in Fig. 4 and the relaxed displacements in Fig. 1, we plot in Fig. 5 the stresses and displacements in the SCB nanowire *after* subtracting the relaxed stresses and displacements. As can be observed, once the relaxed stresses and displacements are removed, the SCB nanowire exhibits bending stresses and displacements similar to those expected from continuum beam theory, and exhibited by the BCB nanowire:  $\sigma_{11}$  exhibits a largely linear pattern within the nanowire bulk, with deviation occurring near the nanowire surfaces,  $\sigma_{12}$  exhibits the expected parabolic pattern, again matching the BCB solution within the nanowire bulk, and deviating near the surface, while the bending displacements again match closely, with the displacement error being about 1.3%. Furthermore, we note that the normal stress  $\sigma_{11}$  is more positive at the bottom of the fixed/fixed nanowire than at the top; this makes sense as the top surface of beams are in compression for bending in a fixed/fixed configuration, while the bottom of the same beam is under tension.

We conclude this section on the nanowire bending stresses and displacements with three comments. First, our results demonstrate that the nanowire bending stresses and displacements are strongly impacted by the residual stress and displacement fields that are present in the nanowire due to surface stress driven relaxation; these results are expected to be quantitatively valid as they were obtained using EAM potentials<sup>50</sup> that are known to underestimate the surface stress by 30–50 % as compared to DFT calculations.<sup>58</sup> Prior works have focused upon predicting size and surface effects on the bending stiffness of the nanowires;<sup>30,39,41–45</sup> we will demonstrate in the next section that, just as deformation induced by surface stresses has a significant effect on the nanowire bending stresses and displacements, the deformation induced by surface stresses also has a significant effect on the elastic properties of the nanowires.

Second, we have demonstrated that the bending stresses and displacements, when the relaxed stresses and displacements due to deformation induced by surface stresses are removed, do follow the expected continuum beam theory solutions, i.e., linear for the normal stress  $\sigma_{11}$  and parabolic for the shear stress  $\sigma_{12}$ , but *only within the nanowire bulk*. At the surfaces, the normal and shear stresses deviate substantially, with dependencies on the boundary condition and the

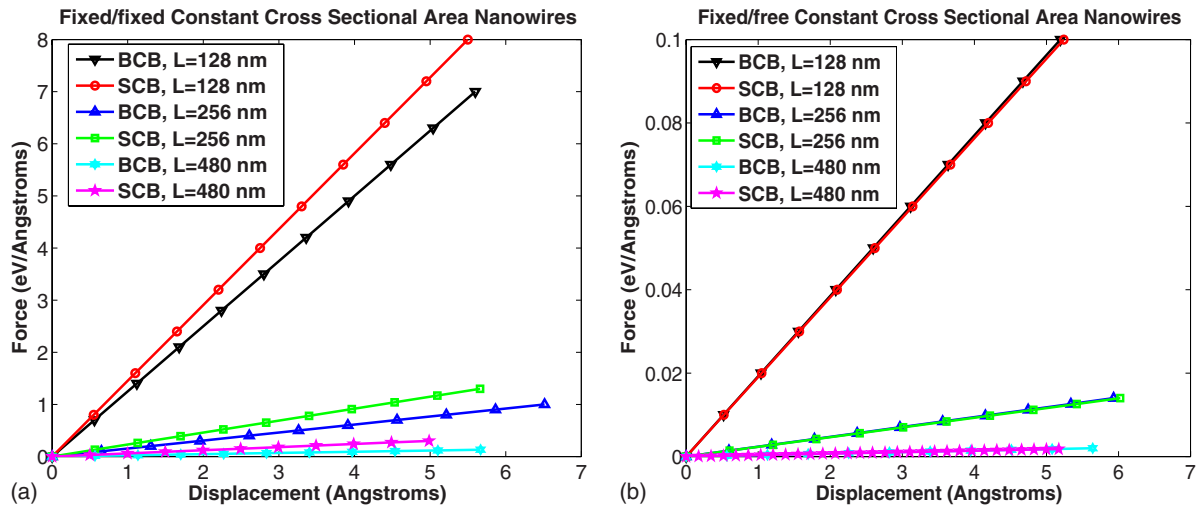


FIG. 6. (Color online) Force versus displacement relationship for CCSA nanowires.

resulting state of deformation due to surface stress driven relaxation.

Finally, we have performed additional simulations which have demonstrated that it is only for very large bending strains, i.e., 5%, where the stresses induced by bending become larger than the stresses induced by surface stress driven relaxation, and only then for fixed/fixed, and not fixed/free nanowires. Because of this factor, and because the bending of the nanowires is likely to occur over much smaller bending strains, the present results are strongly indicative that continuum beam theory solutions cannot be utilized to describe the bending stress state in nanowires that are subject to deformation due to surface stresses.

### VI. NANOWIRE ELASTIC PROPERTIES FROM BENDING SIMULATIONS

The second objective of this work is to characterize the boundary-condition-dependent elastic properties of the nanowires as obtained using the finite element method (FEM) calculations and both the BCB and SCB models; the BCB results are pertinent as they enable us to quantify the effects of surface stresses on the nanowire elastic properties for each geometry considered. To do so, we first show the force vs displacement relationships obtained for the various nanowire geometries and boundary conditions. The force vs displacement relationship is important as it is the quantity that is extracted during experimental measurements of nanowire bending.<sup>8,9,11,12,14</sup>

Through calculation or measurement of the force vs displacement curve, the bending stiffness  $k$  of the nanowires can be directly calculated from

$$\Delta F = k\Delta d, \tag{2}$$

where  $\Delta d$  is the increment in bending displacement that results from the increment in applied force  $\Delta F$ , and  $k$  is the spring constantlike stiffness that relates the force and displacement.

The bending stiffness  $k$  is also a critical parameter because it enables experimentalists to, using the assumptions of

linear elastic continuum beam theory, estimate the nanowire Young's modulus  $E$  using known solutions for fixed/fixed and fixed/free beams, where the stiffness  $k=192EI/L^3$  for a fixed/fixed beam loaded at the beam center, and  $k=3EI/L^3$  for a fixed/free beam loaded at the free end.

We first discuss the results for the elastic properties of CCSA nanowires, where the force vs displacement relationships for fixed/fixed and fixed/free boundary conditions are shown in Fig. 6, and where the calculated bulk-normalized bending stiffness  $k$  and Young's modulus  $E$  for both boundary conditions and all geometries are summarized in Table II.

In analyzing Fig. 6, it is evident that the boundary conditions play a substantial role in the force vs displacement response, and therefore the elastic properties of the nanowires. For the fixed/fixed CCSA nanowires, for all nanowire lengths, more force is required to deform the SCB nanowires to the same displacement as compared to the BCB nanowires of the same size. In contrast, for the fixed/free CCSA nanowires, the force vs displacement plots for the SCB and BCB nanowires are nearly indistinguishable.

The disparities in the force vs displacement response for the two boundary conditions for the CCSA nanowires are highlighted in Table II, where the bulk-normalized bending stiffnesses, and thus Young's modulus for the boundary conditions show very different results. First, Table II demonstrates that Young's modulus for the SCB nanowires shows a slightly decreasing trend with increasing aspect ratio, where the modulus of the fixed/free SCB nanowire is approximately 98% of the bending modulus of the BCB nanowire

TABLE II. Normalized stiffness and Young's modulus, both expressed as a ratio of SCB/BCB, for CCSA nanowires.

Geometry	$\frac{k_{scb}}{k_{bcb}} = \frac{E_{scb}}{E_{bcb}}$ (fixed/free)	$\frac{k_{scb}}{k_{bcb}} = \frac{E_{scb}}{E_{bcb}}$ (fixed/fixed)
$128 \times 16 \times 16$	0.991	1.164
$256 \times 16 \times 16$	0.985	1.497
$384 \times 16 \times 16$	0.983	2.059
$480 \times 16 \times 16$	0.981	2.625

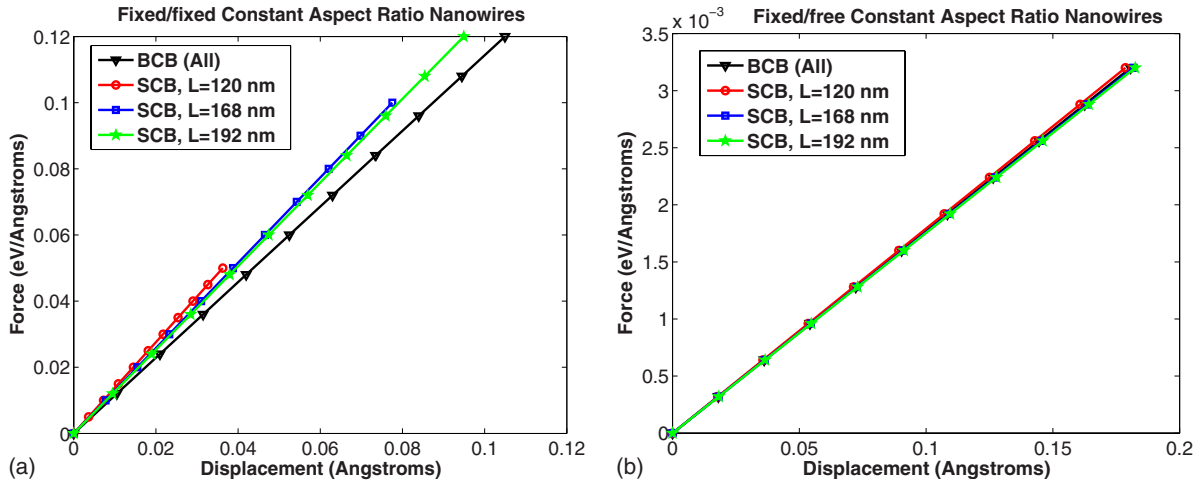


FIG. 7. (Color online) Force versus displacement relationship for CAR nanowires.

when the aspect ratio  $L/a=30$ . The nearly bulk or slightly softened elastic response of fixed/free metal nanowires has been observed both experimentally,<sup>21–23</sup> and using MD simulations.<sup>36</sup>

However, the bending modulus ratio for fixed/fixed nanowires shows a markedly different trend. In particular, the bending modulus for the SCB nanowires increases dramatically as compared to the BCB bending modulus with increasing aspect ratio, with a value more than 2.5 times the BCB value when the aspect ratio  $L/a=30$ . Similar increases in Young’s modulus for fixed/fixed metal nanowires under bending have been found recently by multiple researchers;<sup>10,11</sup> we further discuss our results in comparison with analytic solutions for Young’s modulus that include surface effects from both of those works<sup>10,11</sup> in the next section.

To determine how the variations in the nanowire bending modulus scale with size, we also present the results for the CAR nanowires, which are summarized in Fig. 7 and Table III. The trends for the fixed/free boundary conditions are similar to that observed for the CCSA nanowires, where the force vs displacement response for the SCB and BCB nanowires are nearly indistinguishable. However, again, the SCB nanowires are observed in Fig. 7 to be elastically stiffer than the BCB nanowires of the same size for the fixed/fixed boundary conditions.

Similarly, the bending modulus of the fixed/free SCB nanowires, as shown in Table III, are shown to be nearly indistinguishable from the bending modulus of the BCB nanowires; for all CAR geometries, the SCB bending modulus is only 1% smaller than the BCB bending modulus. In

contrast, the bending modulus of the fixed/fixed SCB nanowires is considerably elevated as compared to the fixed/fixed BCB nanowires. However, Table III also shows the manifestation of how surface effects impact the nanowires with varying size for the CAR nanowires; as the cross-sectional size of the nanowires is increased, the divergence between the SCB and BCB bending moduli begins to diminish, which is expected due to the decrease in overall surface area to volume with increasing nanowire size.

**A. Discussion: Comparison to linear surface-elastic models that account for surface stress and surface stiffness**

We now discuss reasons for the disparity in boundary-condition effects on the nanowire bending stiffness and Young’s modulus. For fixed/fixed silver and lead nanowires, similar increases in both the bending stiffness and Young’s modulus have been observed experimentally by multiple researchers.<sup>10,11</sup> However, we note that the silver and lead nanowires were likely not ideal, defect-free single crystals, and did not have  $\langle 100 \rangle$  axial orientations or  $\{100\}$  transverse surface orientations; for example, the silver nanowires considered by Jing *et al.*<sup>11</sup> were covered with a native oxide layer. This is in contrast to the ideal, defect-free single crystal  $\langle 100 \rangle / \{100\}$  gold nanowires that were studied in this work using the SCB model.

To shed insights into the strengths and limitations of available analytic surface-elastic solutions, we compare the SCB simulation results against those of Jing *et al.*,<sup>11</sup> who used the surface-elastic formulation of Gurtin and Murdoch,<sup>40</sup> which accounts for both surface stress  $\tau_0$  and surface stiffness  $C_0$ , to compare against their experimentally obtained bending stiffness of fixed/fixed silver nanowires. Taking Eq. 17 from Jing *et al.*,<sup>11</sup> and modifying the geometric parameters to account for the fact that our nanowires have a square, and not circular cross section, we obtain an expression for the bulk-normalized Young’s modulus as

$$\left(\frac{E_{\text{eff}}}{E}\right)_{\text{fixed/fixed}} = 1 + \frac{8C_0(1 + \nu^2)}{Ea} + \frac{6L^2\tau_0(1 - \nu)}{5Ea^3}, \quad (3)$$

where  $E_{\text{eff}}$  is the effective Young’s modulus that accounts for surface effects,  $L$  is the nanowire length,  $E$  is the bulk

TABLE III. Normalized stiffness and Young’s modulus, both expressed as a ratio of SCB/BCB, for CAR nanowires.

Geometry	$\frac{k_{\text{scb}}}{k_{\text{hcb}}} = \frac{E_{\text{scb}}}{E_{\text{hcb}}}$ (fixed/free)	$\frac{k_{\text{scb}}}{k_{\text{hcb}}} = \frac{E_{\text{scb}}}{E_{\text{hcb}}}$ (fixed/fixed)
120 × 15 × 15	0.992	1.177
144 × 18 × 18	0.990	1.145
168 × 21 × 21	0.990	1.122
192 × 24 × 24	0.990	1.106

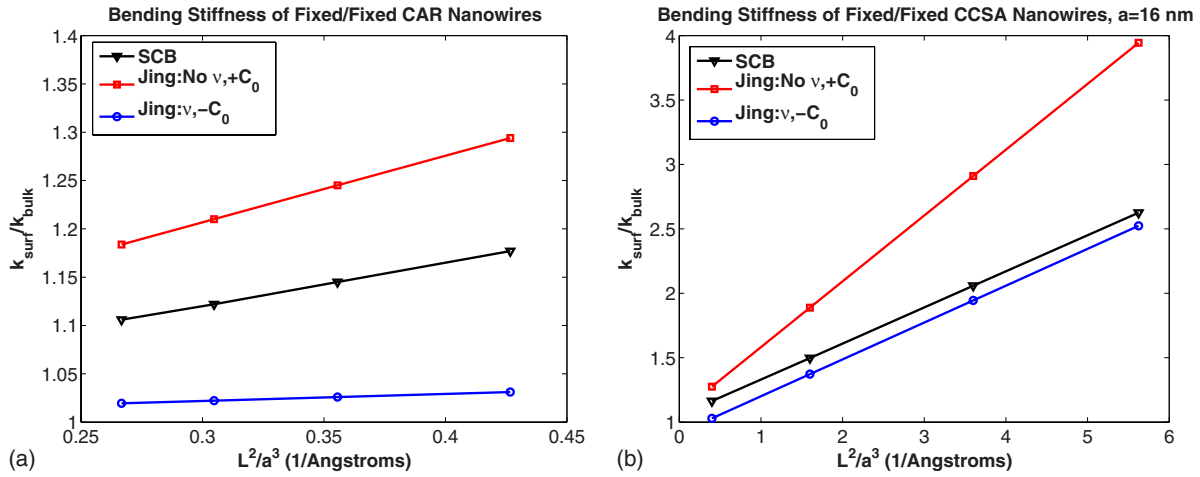


FIG. 8. (Color online) Bulk normalized bending stiffness for fixed/fixed SCB CAR=8 and CCSA nanowires as compared to analytic surface-elastic solutions of Jing *et al.* (Ref. 11) rewritten in Eq. (3).

Young's modulus, and  $a$  is the nanowire cross-sectional length.

Because Jing *et al.*<sup>11</sup> only studied the bending of fixed/fixed nanowires, they did not derive an analytic solution for the effective Young's modulus of fixed/free nanowires. To compare the SCB fixed/free results against the Jing solution, we derive the Jing solution for fixed/free beams in the Appendix, while stating the final result here to be

$$\left(\frac{E_{\text{eff}}}{E}\right)_{\text{fixed/free}} = 1 + \frac{8C_0(1+\nu^2)}{Ea} + \frac{96L^2\tau_0(1-\nu)}{5Ea^3}. \quad (4)$$

For Eqs. (3) and (4), the parameters utilized were  $E = 36$  GPa for  $\langle 100 \rangle$  gold,<sup>50</sup>  $\tau_0 = 0.0981$  eV/ $\text{\AA}^2$ ,<sup>50</sup> and  $C_0 = -0.329$  eV/ $\text{\AA}^2$  (Ref. 59); both the surface stress  $\tau_0$  and surface stiffness  $C_0$  are for  $\{100\}$  gold surfaces, and constitute relaxed values. We additionally note that, unlike the original Jing model,<sup>11</sup> we have accounted for transverse deformation effects by including dependence upon Poisson's ratio  $\nu$  in Eqs. (3) and (4), where  $\nu = 0.44$  for bulk gold.

Due to the geometric factor  $L^2/a^3$  that is present in Eqs. (3) and (4), we plot in Fig. 8 the bulk-normalized bending stiffness (or equivalently the bulk-normalized bending modulus) for the fixed/fixed nanowires as obtained using the SCB and two different Jing models against  $L^2/a^3$ , where two different Jing models were considered for reasons now described.

The (Jing: no  $\nu$ ,  $+C_0$ ) curve in Fig. 8 represents the Jing solution as presented in Eq. 17 of Jing *et al.*;<sup>11</sup> we refer to it in the discussion below as the original Jing model. In that work, transverse deformation was neglected, thus no dependence on Poisson's ratio  $\nu$  was obtained. Furthermore, shear deformation was neglected in the Jing model by assuming that the nanowires had an aspect ratio that exceeded 16. Finally, the surface stiffness  $C_0$  was taken to be positive in the Jing work; this is in contrast to recent atomistic calculations which have shown that  $C_0$  should in fact be negative for most clean FCC metal surfaces,<sup>59,62</sup> as well as for incoherent FCC metal-metal interfaces,<sup>62</sup> though we note that the silver

nanowires considered in the Jing models and experiments were enclosed by an oxide layer.<sup>11</sup>

The (Jing:  $\nu$ ,  $-C_0$ ) curve in Fig. 8 represents the solution of Eq. (3), where transverse deformation is accounted for, and where the surface stiffness  $C_0$  is taken to be negative, with values from Shenoy<sup>59</sup> for  $\{100\}$  gold surfaces. We refer to this as the modified Jing model in the discussion below.

We first observe that while the original Jing model gives reasonable agreement with the SCB results for the CAR=8 nanowires in Fig. 8, the results differ significantly from the SCB results for the CCSA nanowires in Fig. 8. However, if transverse deformation is accounted for and the surface stiffness  $C_0$  is taken to be negative, the modified Jing model agrees very well with the SCB results for the CCSA nanowires in Fig. 8, with improved agreement with increasing aspect ratio, or increasing  $L^2/a^3$ . In contrast, the agreement between the modified Jing model and the SCB results for the CAR=8 geometries is not as good, for reasons discussed below.

The fact that the SCB and modified Jing model have the least accuracy for the smallest aspect ratios is manifested for both small  $L^2/a^3$  for the CCSA nanowires, and also in Fig. 8 for the CAR=8 nanowires. However, because of the improved agreement between the SCB and modified Jing model for the CCSA nanowires with increasing aspect ratio, we also calculated results in Fig. 9 for fixed/fixed CAR nanowires where the aspect ratio was 16 and 24, rather than 8 as seen in Fig. 8; the square cross-sectional length  $a$  was the same as for the CAR=8 nanowires.

In doing so, we find in Fig. 9 very good agreement between the modified Jing model and the CAR nanowires with aspect ratios of 16 and 24, even when the nanowire cross section was the smallest considered in the present work, or  $a = 15$  nm. This finding suggests that nonlinear elastic effects resulting from the reduced nanowire cross-sectional size are not the cause for the difference between the SCB and modified Jing model for the CAR=8 nanowires in Fig. 8, but instead result from the well-known fact that continuum beam theory loses accuracy for smaller aspect ratios, and due to the neglect of shear deformation for short aspect ratio nanowires in the Jing model.

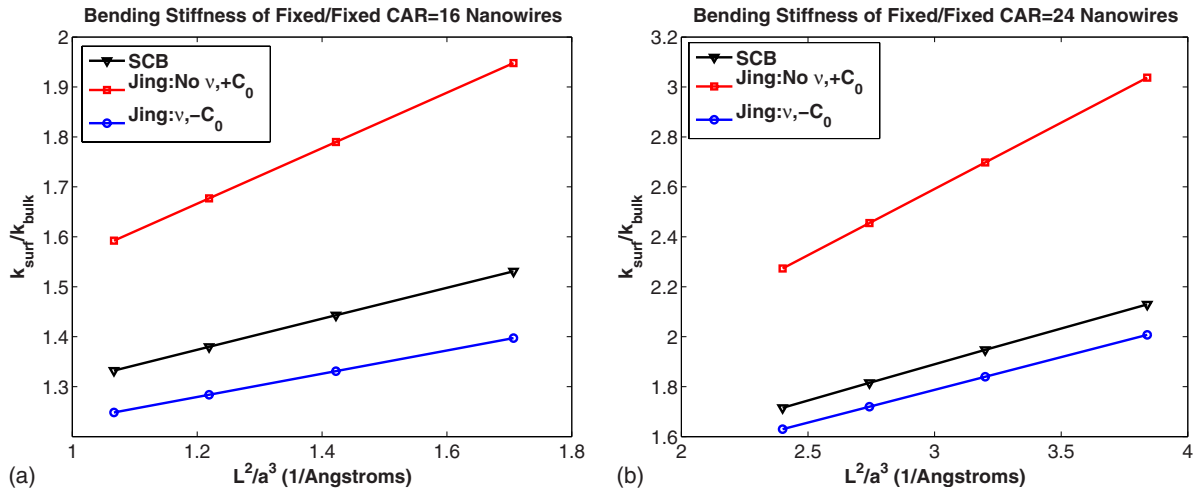


FIG. 9. (Color online) Comparison between SCB results and two different Jing models for CAR nanowires where CAR=16 and CAR=24, with same square nanowire cross-sectional lengths  $a$  as for CAR=8 nanowires discussed earlier.

While there is relatively good agreement for fixed/fixed nanowire bending stiffnesses between the SCB results and the Jing analytic results, they are entirely different for the fixed/free case, as illustrated in Fig. 10 for both nanowire geometries considered. In particular, it is observed that while the original Jing linear surface-elastic analytic solution in Eq. (4) predicts a significant increase in normalized bending stiffness for the fixed/free nanowires, the SCB solution predicts a very slight decrease for both CCSA and CAR geometries. We additionally note that while the modified Jing model reduces the difference as compared to the SCB results, the modified Jing model still predicts that fixed/free nanowires are stiffer than the corresponding bulk material with decreasing nanowire size.

We emphasize that recent atomistic calculations for the bending properties of fixed/free  $\langle 100 \rangle$  silver nanowires with  $\{100\}$  surfaces by McDowell *et al.*<sup>36</sup> also found an essentially bulk response for nanowires with this boundary condition for cross-sectional lengths larger than about 4 nm, while experiments by Petrova *et al.*,<sup>21</sup> Zijlstra *et al.*,<sup>22</sup> and Li *et al.*<sup>23</sup> on

free-standing gold nanowires also showed a slight decrease in the nanowire Young's modulus. We additionally note that in both the Petrova<sup>21</sup> and Zijlstra<sup>22</sup> experimental studies, the nanowires had a  $\langle 100 \rangle$  axial orientation, similar to the SCB nanowires studied in the present work.

The reason why the fixed/free SCB nanowires exhibit different elastic properties under bending than are predicted using the linear Jing surface-elastic solution in Eq. (4) is as follows. Because of the surface stresses, the free end of the nanowire compresses significantly (0.6% or more for the 16 nm cross section CCSA nanowires<sup>48</sup>), which alters the elastic properties of not only the nonlinearly elastic bulk stiffness, but also the nonlinearly elastic surface stiffness, as the SCB model is a nonlinear, finite deformation constitutive model. In particular, compressive strain is known to lead to elastic softening of bulk  $\langle 100 \rangle$  FCC metal crystals;<sup>28,29</sup> therefore, the bulk-elastic softening which results from the surface-stress-driven contraction clearly mitigates the effects of the tensile surface stress for fixed/free nanowires, leading to the slight overall decrease in elastic stiffness as seen in Fig. 10.

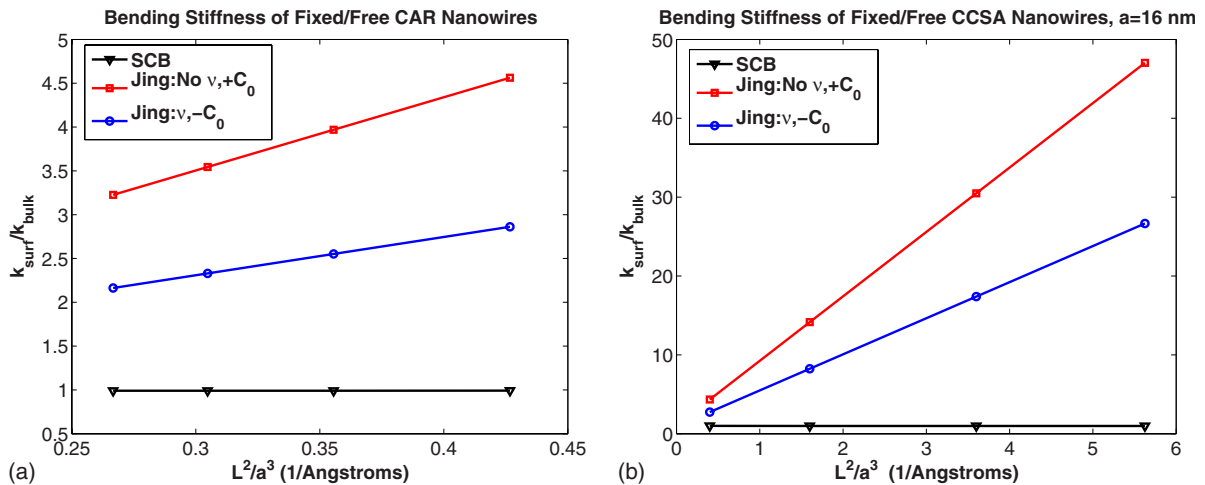


FIG. 10. (Color online) Bulk normalized bending stiffness for fixed/free SCB CAR and CCSA nanowires as compared to the analytic surface-elastic solutions in Eq. (4).

In contrast, both the original and modified Jing surface-elastic bending solutions in Eq. (4) neglect two critical points. First, the compressive relaxation strain that is caused by the surface stresses, and which leads to softening of the  $\langle 100 \rangle$  bulk<sup>28,29</sup> is not accounted for. Second, even if surface-stress-driven compressive strain was captured by Eq. (4), due to the fact that the solutions are based upon linear elasticity, no changes in bulk or surface stiffness due to the deformation would be captured; as seen in Eq. (4), the surface stiffness  $C_0$  is a constant.

Therefore, because the Jing solution in Eq. (4) is based upon the linear surface-elastic theory of Gurtin and Murdoch,<sup>40</sup> and thus depends on both the surface stress  $\tau_0$ , which is generally positive for FCC metals,<sup>59</sup> and the surface stiffness  $C_0$ , which is generally negative for FCC metals,<sup>59</sup> it is realistic as it could possibly predict a decrease in effective modulus due to the presence of the negative surface stiffness  $C_0$ . However, we have shown in the present work that the stiffening effects due to the increase in nanowire length  $L$  which results from the  $L^2/a^3$  term associated with the surface stress  $\tau_0$  in Eq. (4) dominates any softening due to  $C_0$ , and thus a dramatic stiffening is also observed using the Jing solution in Eq. (4) for fixed/free metal nanowires.

### B. Discussion: Comparison to linear surface-elastic models based solely on surface energy

Because there exists a class of analytic linear surface-elastic solutions which depend only on the surface energy  $\gamma$ ,<sup>10,42</sup> and not the surface stress  $\tau_0$  and surface stiffness  $C_0$ , we briefly discuss the implications of the difference form in surface-elastic solution here. One such solution is that given by Cuenot *et al.*,<sup>10</sup>

$$\left( \frac{k_{\text{scb}}}{k_{\text{bulk}}} \right) = 1 + \frac{8L^2\gamma(1-\nu)}{5ED^3}, \quad (5)$$

where  $D$  is the diameter of the nanowire assuming a circular cross section. It is easily seen that, since  $\gamma > 0$  for FCC metals, the Cuenot analytic solution in Eq. (5) can only lead to an increase in Young's modulus with decreasing size. While we also note that Eq. (5) was derived for fixed/fixed nanowires, a similar expression can be derived for fixed/free nanowires, which in contrast to available experimental studies<sup>21-23</sup> and the present SCB results, again guarantees an increase in Young's modulus with decreasing size for fixed/free nanowires.

To further illustrate the importance of nonlinear kinematics in accounting for deformation-induced changes due to surface stresses on the bulk and surface stiffness of nanostructures, we also discuss the analytic solution for nano-beam bending of Guo and Zhao,<sup>42</sup> where relaxation and deformation due to surface stresses are accounted for; however, the surface and bulk constitutive response in that work<sup>42</sup> is linear elastic, so that no changes in material stiffness occur due to the surface stress driven relaxation. In particular, their Eq. 28 gives an expression for the effective Young's modulus accounting for surface relaxation effects as

$$E_{\text{eff}} = E_{\text{bulk}} + \frac{\gamma L^2(1-\nu)}{(N+2nk)^3 a^3}, \quad (6)$$

where  $k$  is the surface relaxation parameter, which is a positive number chosen to vary between 0.85 and 1.15; we note the similarity of this expression to Eq. (5). However, because the surface relaxation parameter  $k > 0$  and because the surface energy  $\gamma > 0$ , the effective Young's modulus described by Eq. (6) must stiffen with decreasing nanowire cross-sectional size  $a$  for both fixed/fixed and fixed/free boundary conditions.

This is again in contrast, for fixed/free boundary conditions, to the SCB results obtained in the present work, recent atomistic simulations,<sup>36</sup> and recent resonant experiments on gold nanowires,<sup>21,22</sup> all of which predict slight decreases in  $\langle 100 \rangle$  gold nanowire Young's modulus for fixed/free or free-standing boundary conditions.

It is worth emphasizing that while previous computational studies of metal nanowires have found a reduced elastic modulus due to surface stress effects,<sup>28,29,51</sup> the present finding that softening of fixed/free nanowires can occur despite the presence of surface stresses has not been found by previous researchers,<sup>10,11,42,44,45</sup> mainly due to the fact that the analytic works have considered fixed/fixed boundary conditions only.

The present results strongly indicate that a combination of key factors, including boundary conditions and changes in both surface- and bulk-elastic properties due to surface stress driven relaxation, must be accounted for to accurately predict the boundary-condition-dependent bending-derived elastic properties of metal nanowires that are subject to surface stresses.

### C. Discussion: Comparison of nanowire Young's modulus from bending and resonance SCB calculations

We conclude our analysis by presenting a comparison between Young's modulus of the metal nanowires as computed in the present work using bending simulations, and SCB resonance simulations of the nanowire Young's modulus as previously described by Park and Klein.<sup>51</sup> An analysis of Young's modulus that might be expected from different loading methods is critical due to the fact that experimentally, bending and resonance of nanowires are the two most common methods to extract, by using continuum beam theory relationships, Young's modulus of the nanowires.

For the SCB resonance calculations, we first calculated the resonant frequencies through solution of a standard finite element eigenvalue problem, where the FEM stiffness matrix is the relaxed stiffness matrix after deformation due to surface stresses. After obtaining the resonant frequencies, the nanowire Young's modulus was obtained by relating the resonant frequencies to Young's modulus using standard continuum beam theory expressions.<sup>63</sup>

The comparison of the fixed/fixed CCSA and CAR nanowires are shown in Fig. 11. In all figures, we plot the bulk-normalized Young's modulus against the inverse length ratio  $L^2/a^3$ , in accordance with the analytic solutions for bending in Eqs. (3) and (4). As can be seen in Fig. 11, the bulk-

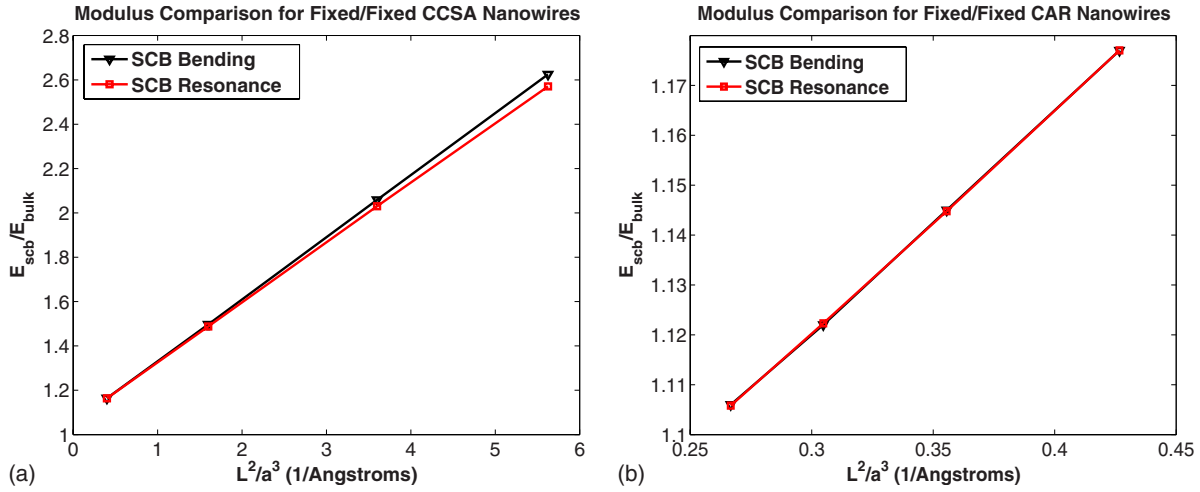


FIG. 11. (Color online) Comparison of nanowire Young’s modulus obtained from SCB bending and resonance calculations for fixed/fixed CCSA and CAR nanowires.

normalized Young’s modulus for fixed/fixed boundary conditions is found to be nearly identical whether bending or resonance calculations are performed, for both CAR and CCSA nanowires.

We show in Fig. 12 the comparison of the bulk-normalized Young’s modulus for the fixed/free CCSA and CAR nanowires. Again, very little discrepancy between Young’s modulus obtained via resonance or via bending is found, where both the SCB bending and resonance calculations predict a very slight decrease in nanowire Young’s modulus as compared to the bulk value for both CAR and CCSA geometries. We note again the agreement with recent experimental results showing the same trend for fixed/free or free standing gold nanowires.<sup>21–23</sup> The present results collectively indicate that surface stresses have a similar effect on the elastic properties of nanowires as measured using either resonance or bending testing techniques.

VII. CONCLUSIONS

In conclusion, we have utilized the surface Cauchy-Born model to quantify the effects of surface stresses on the bend-

ing behavior and properties of  $\langle 100 \rangle$  gold nanowires with  $\{100\}$  transverse surfaces. By studying the bending behavior and properties of nanowires accounting for both fixed/fixed and fixed/free boundary conditions, we have found that: (1) in agreement with available experimental data, Young’s modulus of the nanowires varies depending on the boundary condition; a distinct stiffening was found for fixed/fixed boundary conditions,<sup>10,11</sup> while a very slight softening was found for fixed/free boundary conditions.<sup>21–23</sup> (2) The stresses in the nanowires resulting from surface stress-induced deformation, for both boundary conditions, are significantly larger than the stresses generated through bending unless very large bending strains ( $\approx 5\%$ ) are reached. (3) The displacements along the nanowire cross section due to surface stress induced deformation are also on the same order as the deformations due to bending unless large ( $>1\%$ ) bending strains are generated. (4) Because of the magnitude of the stresses and displacements in the nanowires induced by surface stresses in the absence of applied bending forces, continuum beam theories for bending do not appear to be applicable in describing the stresses and displacements of nanowires. (5) Analytic solutions in the literature that are

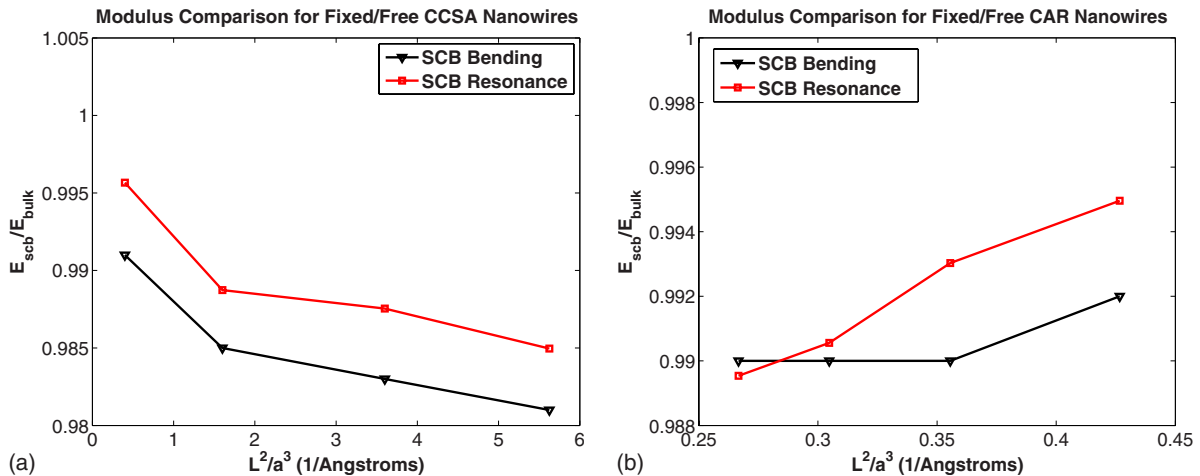


FIG. 12. (Color online) Comparison of nanowire Young’s modulus from SCB bending and resonance calculations for fixed/free CCSA and CAR nanowires.

derived from linear surface-elastic theory were found to give markedly different predictions for Young's modulus of nanowires obtained from bending. While Young's modulus obtained from SCB simulations was found to be similar to analytic solutions for fixed/fixed nanowires, analytic solutions for fixed/free nanowires predicted a significant increase in Young's modulus, while a slight decrease was found in both experiments<sup>21-23</sup> and also the SCB simulations. (6) It was found that analytic surface-elastic solutions that are based only on the surface energy  $\gamma$ , such as that of Cuenot *et al.*<sup>10</sup> and Guo and Zhao,<sup>42</sup> must lead to a predicted stiffening of the nanowire regardless of boundary condition due to the fact that  $\gamma > 0$ . In contrast, analytic surface-elastic solutions such as that of Jing *et al.*<sup>11</sup> which incorporate surface stress and stiffness following Gurtin and Murdoch,<sup>40</sup> can theoretically predict softening due to the presence of the negative surface stiffness. However, we have shown that the stiffening effects of the surface stress dominate the softening due to the surface stiffness for the range of geometries considered in the present work. (7) An additional shortcoming of linear surface-elastic analytic solutions arises from their inability to capture softening or stiffening of the nanowire bulk due to deformation induced by surface stresses; these effects arise naturally out of the finite deformation SCB model, and were shown to be critical in predicting the slight softening of fixed/free nanowires that is observed experimentally. (8) Surface stress effects were found to have a similar effect on the elastic properties of nanowires for both SCB bending and resonance calculations.

#### ACKNOWLEDGMENTS

H.S.P. and G.Y. both acknowledge support of the NSF through Grant No. CMMI-0750395; G.Y. also acknowledges support from the University of Colorado. Both authors also acknowledge the assistance of Patrick Klein with the surface stress output in Tahoe, and the helpful comments of the reviewer.

#### APPENDIX: DERIVATION FOR FIXED/FREE JING LINEAR SURFACE-ELASTIC EQUATIONS

We derive in this appendix the equivalent expression for Eqs. 16 and 17 in Jing *et al.*<sup>11</sup> for the case of fixed/free nanowires. For fixed/free nanowires, because the extension of the beam  $\Delta L$  can be calculated to be

$$\Delta L = \frac{1}{2} \int_0^L y'(x)^2 dx = \frac{3\delta^2}{5L}, \quad (\text{A1})$$

we obtain the strain of the neutral axis as

$$\epsilon_0 = \frac{3\delta^2}{5L^2}, \quad (\text{A2})$$

where  $\delta$  is the deflection of the free end and  $L$  is the length of the nanowire. The normal strain along the square cross section of the beam is then

$$\epsilon_{xx} = \epsilon_0 + \frac{y}{\rho}, \quad (\text{A3})$$

where the radius of the curvature of the nanowire is

$$\rho = \frac{L^3}{3\delta(x-L)}. \quad (\text{A4})$$

Similar to Eq. 13 in Jing *et al.*,<sup>11</sup> the surface strain energy can be written as, assuming a square nanowire cross section,

$$U_s = \int \int_{\text{Surface}} \left( \tau_0 \epsilon_{xx} + \frac{1}{2} \mathbf{C}_0 \epsilon_{xx}^2 \right) ds = 4aL\tau_0\epsilon_0 + 2aL\mathbf{C}_0\epsilon_0^2 + \frac{\mathbf{C}_0 a^3 \delta^2}{L^3}, \quad (\text{A5})$$

where  $\tau_0$  is the surface stress when  $\epsilon_{xx}=0$ ,  $a$  is the cross-sectional length of the square cross section, and  $\mathbf{C}_0$  is the surface-elastic modulus.

Similar to Eq. 14 in Jing *et al.*,<sup>11</sup> the bulk-elastic energy  $U_b$  of the nanowire can be written as, again assuming a square cross section,

$$U_b = \int \int \int_{\text{Volume}} \frac{1}{2} E \epsilon_{xx}^2 dv = \frac{1}{2} a^2 L E \epsilon_0^2 + \frac{a^4 E \delta^2}{8L^3}, \quad (\text{A6})$$

where  $E$  is the bulk Young's modulus. Then, similar to Eq. 15 in Jing *et al.*,<sup>11</sup> the total elastic energy  $U$  of the homogeneous nanowire with an apparent Young's modulus  $E_{\text{eff}}$  is written as

$$U = \int \int \int_{\text{Volume}} \frac{1}{2} E_{\text{eff}} \epsilon_{xx}^2 dv = \frac{1}{2} a^2 L E_{\text{eff}} \epsilon_0^2 + \frac{a^4 E_{\text{eff}} \delta^2}{8L^3}, \quad (\text{A7})$$

By applying the relation  $U = U_s + U_b$ , we obtain

$$E_{\text{eff}} = E + \frac{8\mathbf{C}_0}{a} + \frac{12\tau_0 L^2}{5a^3 \left( \frac{1}{8} + \frac{9\delta^2}{50a^2} \right)} - \frac{18 \left( \frac{\delta}{a} \right)^2 \mathbf{C}_0}{25a \left( \frac{1}{8} + \frac{9\delta^2}{50a^2} \right)}, \quad (\text{A8})$$

which is the equivalent expression to Eq. 16 in Jing *et al.*,<sup>11</sup> though assuming a square cross section and fixed/free boundary conditions. If we further assume that  $\delta/a \ll 1$ , Eq. (A8) can be written as

$$\left( \frac{E_{\text{eff}}}{E} \right)_{\text{fixed/free}} = 1 + \frac{8\mathbf{C}_0}{aE} + \frac{96L^2\tau_0}{5a^3E}. \quad (\text{A9})$$

When the Poisson effect due to transverse deformation is accounted for, the nonzero strain components should include  $\epsilon_{yy} = -\nu\epsilon_{xx}$  and  $\epsilon_{zz} = -\nu\epsilon_{xx}$ . This leads to a new surface strain energy which takes the Poisson effect into account, and takes the following form

$$U_s = 4aL(1-\nu)\tau_0\epsilon_0 + 2aL(1+\nu^2)\mathbf{C}_0\epsilon_0^2 + \frac{\mathbf{C}_0 a^3 (1+\nu^2) \delta^2}{L^3}. \quad (\text{A10})$$

The bulk-elastic energy  $U_b$  and the total elastic energy  $U$  do not change. By the same procedure, we can rewrite Eqs. (A8) and (A9) as

$$E_{\text{eff}} = E + \frac{8(1 + \nu^2)C_0}{a} + \frac{12\tau_0(1 - \nu)L^2}{5a^3\left(\frac{1}{8} + \frac{9\delta^2}{50a^2}\right)} - \frac{18\left(\frac{\delta}{a}\right)^2(1 + \nu^2)C_0}{25a\left(\frac{1}{8} + \frac{9\delta^2}{50a^2}\right)}, \quad (\text{A11})$$

and

$$\left(\frac{E_{\text{eff}}}{E}\right)_{\text{fixed/free}} = 1 + \frac{8C_0}{aE}(1 + \nu^2) + \frac{96L^2(1 - \nu)\tau_0}{5a^3E}. \quad (\text{A12})$$

\*harold.park@colorado.edu

- <sup>1</sup>Y. Xia, P. Yang, Y. Sun, Y. Wu, B. Mayers, B. Gates, Y. Yin, F. Kim, and H. Yan, *Adv. Mater.* **15**, 353 (2003).
- <sup>2</sup>C. M. Lieber and Z. L. Wang, *MRS Bull.* **32**, 99 (2007).
- <sup>3</sup>H. S. Park, W. Cai, H. D. Espinosa, and H. Huang, *MRS Bull.* **34**, 178 (2009).
- <sup>4</sup>H. G. Craighead, *Science* **290**, 1532 (2000).
- <sup>5</sup>N. V. Lavrik, M. J. Sepaniak, and P. G. Datskos, *Rev. Sci. Instrum.* **75**, 2229 (2004).
- <sup>6</sup>K. L. Ekinici and M. L. Roukes, *Rev. Sci. Instrum.* **76**, 061101 (2005).
- <sup>7</sup>E. W. Wong, P. E. Sheehan, and C. M. Lieber, *Science* **277**, 1971 (1997).
- <sup>8</sup>B. Wu, A. Heidelberg, and J. J. Boland, *Nature Mater.* **4**, 525 (2005).
- <sup>9</sup>A. Heidelberg, L. T. Ngo, B. Wu, M. A. Phillips, S. Sharma, T. I. Kamins, J. E. Sader, and J. J. Boland, *Nano Lett.* **6**, 1101 (2006).
- <sup>10</sup>S. Cuenot, C. Fréty, S. Demoustier-Champagne, and B. Nysten, *Phys. Rev. B* **69**, 165410 (2004).
- <sup>11</sup>G. Y. Jing, H. L. Duan, X. M. Sun, Z. S. Zhang, J. Xu, Y. D. Li, J. X. Wang, and D. P. Yu, *Phys. Rev. B* **73**, 235409 (2006).
- <sup>12</sup>S. Hoffmann, I. Utke, B. Moser, J. Michler, S. H. Christiansen, V. Schmidt, S. Senz, P. Werner, U. Gosele, and C. Ballif, *Nano Lett.* **6**, 622 (2006).
- <sup>13</sup>Y. Chen, B. L. Dorgan, D. N. McIlroy, and D. E. Aston, *J. Appl. Phys.* **100**, 104301 (2006).
- <sup>14</sup>A. San Paulo, J. Bokor, R. T. Howe, R. He, P. Yang, D. Gao, C. Carraro, and R. Maboudian, *Appl. Phys. Lett.* **87**, 053111 (2005).
- <sup>15</sup>D. A. Dikin, X. Chen, W. Ding, G. Wagner, and R. S. Ruoff, *J. Appl. Phys.* **93**, 226 (2003).
- <sup>16</sup>S. S. Verbridge, J. M. Parpia, R. B. Reichenbach, L. M. Bellan, and H. G. Craighead, *J. Appl. Phys.* **99**, 124304 (2006).
- <sup>17</sup>X. Li, T. Ono, Y. Wang, and M. Esashi, *Appl. Phys. Lett.* **83**, 3081 (2003).
- <sup>18</sup>A. Husain, J. Hone, H. W. C. Postma, X. M. H. Huang, T. Drake, M. Barbic, A. Scherer, and M. L. Roukes, *Appl. Phys. Lett.* **83**, 1240 (2003).
- <sup>19</sup>C. Y. Nam, P. Jaroenapibal, D. Tham, D. E. Luzzi, S. Evoy, and J. E. Fischer, *Nano Lett.* **6**, 153 (2006).
- <sup>20</sup>C. Q. Chen, Y. Shi, Y. S. Zhang, J. Zhu, and Y. J. Yan, *Phys. Rev. Lett.* **96**, 075505 (2006).
- <sup>21</sup>H. Petrova, J. Perez-Juste, Z. Y. Zhang, J. Zhang, T. Kosel, and G. V. Hartland, *J. Mater. Chem.* **16**, 3957 (2006).
- <sup>22</sup>P. Zijlstra, A. L. Tchebotareva, J. W. M. Chon, M. Gu, and M. Orrit, *Nano Lett.* **8**, 3493 (2008).
- <sup>23</sup>M. Li, T. S. Mayer, J. A. Sioss, C. D. Keating, and R. B. Bhiladvala, *Nano Lett.* **7**, 3281 (2007).
- <sup>24</sup>R. C. Cammarata, *Prog. Surf. Sci.* **46**, 1 (1994).
- <sup>25</sup>J. Diao, K. Gall, and M. L. Dunn, *Nature Mater.* **2**, 656 (2003).
- <sup>26</sup>H. S. Park, K. Gall, and J. A. Zimmerman, *Phys. Rev. Lett.* **95**, 255504 (2005).
- <sup>27</sup>W. Liang, M. Zhou, and F. Ke, *Nano Lett.* **5**, 2039 (2005).
- <sup>28</sup>L. G. Zhou and H. Huang, *Appl. Phys. Lett.* **84**, 1940 (2004).
- <sup>29</sup>H. Liang, M. Upmanyu, and H. Huang, *Phys. Rev. B* **71**, 241403(R) (2005).
- <sup>30</sup>R. Dingreville, J. Qu, and M. Cherkaoui, *J. Mech. Phys. Solids* **53**, 1827 (2005).
- <sup>31</sup>C. Q. Sun, B. K. Tay, X. T. Zeng, S. Li, T. P. Chen, J. Zhou, H. L. Bai, and E. Y. Jiang, *J. Phys.: Condens. Matter* **14**, 7781 (2002).
- <sup>32</sup>J. Q. Broughton, F. F. Abraham, N. Bernstein, and E. Kaxiras, *Phys. Rev. B* **60**, 2391 (1999).
- <sup>33</sup>J. Q. Broughton, C. A. Meli, P. Vashishta, and R. K. Kalia, *Phys. Rev. B* **56**, 611 (1997).
- <sup>34</sup>B. Lee and R. E. Rudd, *Phys. Rev. B* **75**, 195328 (2007).
- <sup>35</sup>R. E. Rudd, *Int. J. Multiscale Comp. Eng.* **2**, 203 (2004).
- <sup>36</sup>M. T. McDowell, A. M. Leach, and K. Gall, *Modell. Simul. Mater. Sci. Eng.* **16**, 045003 (2008).
- <sup>37</sup>M. A. Makeev, D. Srivastava, and M. Menon, *Phys. Rev. B* **74**, 165303 (2006).
- <sup>38</sup>P. A. T. Olsson, S. Melin, and C. Persson, *Phys. Rev. B* **76**, 224112 (2007).
- <sup>39</sup>R. E. Miller and V. B. Shenoy, *Nanotechnology* **11**, 139 (2000).
- <sup>40</sup>M. E. Gurtin and A. Murdoch, *Arch. Ration. Mech. Anal.* **57**, 291 (1975).
- <sup>41</sup>J. Zang and F. Liu, *Appl. Phys. Lett.* **92**, 021905 (2008).
- <sup>42</sup>J.-G. Guo and Y.-P. Zhao, *Nanotechnology* **18**, 295701 (2007).
- <sup>43</sup>C. W. Lim and L. H. He, *Int. J. Mech. Sci.* **46**, 1715 (2004).
- <sup>44</sup>H. X. Zhu and B. L. Karihaloo, *Int. J. Plast.* **24**, 991 (2008).
- <sup>45</sup>P. Lu, L. H. He, H. P. Lee, and C. Lu, *Int. J. Solids Struct.* **43**, 4631 (2006).
- <sup>46</sup>J. He and C. M. Lilley, *Nano Lett.* **8**, 1798 (2008).
- <sup>47</sup>H. S. Park, P. A. Klein, and G. J. Wagner, *Int. J. Numer. Methods Eng.* **68**, 1072 (2006).
- <sup>48</sup>H. S. Park and P. A. Klein, *Phys. Rev. B* **75**, 085408 (2007).
- <sup>49</sup>M. S. Daw and M. I. Baskes, *Phys. Rev. B* **29**, 6443 (1984).
- <sup>50</sup>S. M. Foiles, M. I. Baskes, and M. S. Daw, *Phys. Rev. B* **33**, 7983 (1986).

- <sup>51</sup>H. S. Park and P. A. Klein, *J. Mech. Phys. Solids* **56**, 3144 (2008).
- <sup>52</sup>E. Tadmor, M. Ortiz, and R. Phillips, *Philos. Mag. A* **73**, 1529 (1996).
- <sup>53</sup>M. Arroyo and T. Belytschko, *J. Mech. Phys. Solids* **50**, 1941 (2002).
- <sup>54</sup>P. Zhang, Y. Huang, P. H. Geubelle, P. A. Klein, and K. C. Hwang, *Int. J. Solids Struct.* **39**, 3893 (2002).
- <sup>55</sup>H. S. Park and P. A. Klein, *Comput. Methods Appl. Mech. Eng.* **197**, 3249 (2008).
- <sup>56</sup>Z. Tang, H. Zhao, G. Li, and N. R. Aluru, *Phys. Rev. B* **74**, 064110 (2006).
- <sup>57</sup>E. B. Tadmor, G. S. Smith, N. Bernstein, and E. Kaxiras, *Phys. Rev. B* **59**, 235 (1999).
- <sup>58</sup>J. Wan, Y. L. Fan, D. W. Gong, S. G. Shen, and X. Q. Fan, *Modell. Simul. Mater. Sci. Eng.* **7**, 189 (1999).
- <sup>59</sup>V. B. Shenoy, *Phys. Rev. B* **71**, 094104 (2005).
- <sup>60</sup>H. S. Park, *Nanotechnology* **20**, 115701 (2009).
- <sup>61</sup>Tahoe, <http://tahoe.ca.sandia.gov> (2008).
- <sup>62</sup>C. Mi, S. Jun, D. A. Kouris, and S. Y. Kim, *Phys. Rev. B* **77**, 075425 (2008).
- <sup>63</sup>W. Weaver, S. P. Timoshenko, and D. H. Young, *Vibration Problems in Engineering* (Wiley, New York, 1990).